ISSN 0006-2979, Biochemistry (Moscow), 2024, Vol. 89, No. 3, pp. 474-486 © Pleiades Publishing, Ltd., 2024.

# Effect of Focal Adhesion Kinase and Vinculin Expression on Migration Parameters of Normal and Tumor Epitheliocytes

**Evgenia S. Solomatina[1,2], Anastasia V. Kovaleva[1,2], Anna V. Tvorogova[1,3], Ivan A. Vorobjev[1], and Aleena A. Saidova[1,2,a]***

[1]*Lomonosov Moscow State University, Department of Biology, 119991 Moscow, Russia*
[2]*Engelhardt Institute of Molecular Biology, Russian Academy of Sciences, 119991 Moscow, Russia*
[3]*Belozersky Research Institute of Physico-Chemical Biology, 119991 Moscow, Russia*
[a]*e-mail: aleena.saidova@gmail.com*

Received November 17, 2023
Revised January 11, 2024
Accepted January 17, 2024

**Abstract**—Focal adhesions (FAs) are mechanosensory structures that transform physical stimuli into chemical signals guiding cell migration. Comprehensive studies postulate correlation between the FA parameters and cell motility metrics for individual migrating cells. However, which properties of the FAs are critical for epithelial cell motility in a monolayer remains poorly elucidated. We used high-throughput microscopy to describe relationship between the FA parameters and cell migration in immortalized epithelial keratinocytes (HaCaT) and lung carcinoma cells (A549) with depleted or inhibited vinculin and focal adhesion kinase (FAK) FA proteins. To evaluate relationship between the FA morphology and cell migration, we used substrates with varying stiffness in the model of wound healing. Cells cultivated on fibronectin had the highest FA area values, migration rate, and upregulated expression of FAK and vinculin mRNAs, while the smallest FA area and slower migration rate to the wound were specific to cells cultivated on glass. Suppression of vinculin expression in both normal and tumor cells caused decrease of the FA size and fluorescence intensity but did not affect cell migration into the wound. In contrast, downregulation or inactivation of FAK did not affect the FA size but significantly slowed down the wound closure rate by both HaCaT and A549 cell lines. We also showed that the FAK knockdown results in the FA lifetime decrease for the cells cultivated both on glass and fibronectin. Our data indicate that the FA lifetime is the most important parameter defining migration of epithelial cells in a monolayer. The observed change in the cell migration rate in a monolayer caused by changes in expression/activation of FAK kinase makes FAK a promising target for anticancer therapy of lung carcinoma.

**DOI**: 10.1134/S0006297924030088

*Keywords*: focal adhesions, vinculin, FAK kinase, lung cancer adenocarcinoma, wound healing assay, migration

## INTRODUCTION

Focal adhesions (FAs) are large multiprotein structures that transform physical cues from extracellular matrix into chemical signals inside the cell and thus regulate cell motility. Due to their key role in signal transduction and force transmission, FAs are essential for all types of cell motility, including 2D migration on a substrate [1].

The structure of FAs ubiquitous among different cell types includes three distinct layers: the bottom integrin signaling layer, the force transduction layer, and the regulatory layer with actin binding proteins [2-4]. Focal adhesion kinase (FAK) is located at the bottom

*Abbreviations*: A549, human lung adenocarcinoma cells; ECM, extracellular matrix; FAs, focal adhesions; FAK, focal adhesion kinase; HaCaT, immortalized human epithelial keratinocytes, RFP, red fluorescent protein.

* To whom correspondence should be addressed.

layer and serves as one of the key signaling proteins both due to its kinase activity and scaffolding properties [5]. Upon recruitment and activation of paxillin to FA site, FAK kinase interacts with paxillin and binds talin [6, 7], after which these proteins begin to work as an interactive platform for assembly of mature FA [8]. In cancer cells FAK plays essential role in metastases formation via promoting cell migration and invasion. Overexpression of FAK as well as its functional activation positively correlate with metastasis rate, poor prognosis, and survival [9-11]. Numerous reports indicate that FAK facilitates cancer cell survival and proliferation and regulates cancer cell metabolism, thus enhancing not only cell migration and invasion, but also other tumor-promoting processes [12-15].

Dynamics of FAs is also defined by the substrate stiffness and composition. Cells on the stiff substrates have larger FAs with increased expression of key regulatory and structural molecules like paxillin, vinculin, or zyxin [16-19], whereas on the 2D substrates with reduced stiffness or in the soft 3D gels FAs are typically smaller [20, 21]. Comprehensive studies confirm correlation between the focal adhesion size and cell motility for several types of cells such as single fibroblasts or myoblasts [22, 23]. However, whether the change in the FA parameters that occurs in response to the substrate cues from extracellular matrix (ECM) or altered expression of the FA proteins affects migration of normal and cancer cells, remains poorly understood. Here we use high-throughput microscopy to describe functional relationship between the focal adhesion descriptors and cell migration parameters by changing the substrate stiffness and altering expression or inhibiting the FA proteins in the immortalized human epithelial keratinocytes (HaCaT) and lung carcinoma cells (A549). In this study we for the first time show that the FAK depletion in normal and cancer keratinocytes moving in a monolayer leads to the statistically significant decrease in the FA lifetime and slows down directed cell motility in a wound healing assay.

## MATERIALS AND METHODS

**Cell lines.** A549 (lung carcinoma) and HaCaT (normal human keratinocytes) cells were obtained from the American Type Culture Collection (USA) and cultured in a DMEM/F12 medium (PanEco, Russia) supplemented with 10% of fetal bovine serum (PanEco) and 0.8 mg/ml gentamycin at 37°C under 5% $CO_2$.

**Plastic coating.** Coating of wells with fibronectin, vitronectin, or poly-D-lysine (Sigma-Aldrich, USA) was performed at concentration 5 μg/cm$^2$; the wells were coated with 150 μl of solution for 1 h at 37°C, then the wells were air-dried under sterile conditions.

**Wound healing assay.** Cells were plated in 6-well plates and grown to full confluence. The cell layer was scratched by a tip of sterile 10-μl pipette (width ~350 μm). Cell debris was removed by washing twice with a DMEM serum-free medium, and cells migrated into the wound were imaged using time-lapse microscopy during the following 600 min. Live imaging was carried out with an inverted Zeiss AxioObserver fluorescence microscope with ×20/1.6 objective (phase contrast) operating under control of the Zen 3.1 Blue Edition software at 36.5-37°C in $CO_2$-independent medium (Gibco, USA) using a Hamamatsu ORCA-Flash4.0 V2 camera (Hamamatsu Photonics, Japan) with 10-minute intervals between the frames. Each well had 6 scratches and the experiment was repeated three times. Each measurement was made according to the method described by Kauanova et al. [24] using ImageJ software.

**RNA interference.** A549 lung cancer cells were transfected with the FAK siRNA, vinculin siRNA, or control non-specific siRNA (to GFP) using a TurboFect™ (Thermo Fisher Scientific, USA) transfection reagent according to the manufacturer's instructions. Briefly, cells in 35-mm Petri dishes were grown to 65% confluence and transfected with 100 pmol siRNA per well (volume ratio of transfection reagent to siRNA 3 : 1), after 12 h of incubation the medium with transfection complexes was replaced with a fresh one. All siRNA sequences were designed using free BLOCK-IT software (https://rnaidesigner.thermofisher.com/rnaiexpress/) and purchased from DNA-Synthesis (Russia). Sequences for each siRNA are provided in Table S1 in the Online Resource 1.

**RNA isolation and reverse transcription.** RNA was extracted from cell suspensions using a RNeasy Mini Kit (Qiagen, USA) according to the manufacturer's instructions. RNA concentration was measured using a NanoPhotometer (Implen, Germany) and its purity was assessed based on the A260/A280 and A260/A230 absorbance ratios. cDNA was transcribed using an iScript Advanced cDNA synthesis kit (Bio-Rad, USA) according to the manufacturer's instructions, 500 ng of total RNA was taken into reaction.

**Real-time qPCR.** Real-time qPCR was performed with a CFX96 (Bio-Rad) cycler. Relative amounts of mRNA were determined using an iTaq Universal SYBR Green Supermix (Bio-Rad). The reaction protocol included denaturation (95°C, 10 min), followed by 39 amplification cycles (95°C, 15 s; X°C (exact annealing temperature for each primer pair is provided in Table S2 in the Online Resource 1), 30 s; and 72°C, 60 s). All samples were processed in triplicate. One sample of cDNA put into each qPCR run served as an inter-run calibrator for combining data into one experiment. Primer sequences are provided in Table S2 in the Online Resource 1. Primers were purchased from DNA-Synthesis. Primer specificity was confirmed by melting curve analysis.

Ct values were determined for real-time qPCR curves by setting threshold at 5 SD for each run. qPCR data were normalized according to Vandesompele et al. [25] using UBC and HPRT1 as reference genes.

**Characterization of stable HaCaT and A549 cell lines.** To obtain HaCaT and A549 cell lines with stable expression of RFP (red fluorescent protein)-conjugated vinculin, we cloned vinculin cDNA into pSLIK lentiviral vector containing RFP gene as a reporter and puromycin resistance gene as a selection marker (Evrogen, Russia). The lentiviral vector was co-transfected into HEK293 packaging cells (American Type Culture Collection, ATCC #CRL-11268) with X-tremeGENE HP DNA transfection reagent according to the manufacturer's protocol. Released viruses were harvested 24 and 48 h after transfection and next used for transduction of A549 and HaCaT cells. Virus titer was determined in serial dilution experiments of viral particles added to $6\times10^5$ HEK293T cells seeded on a 12-well plate 24 h before transduction. Polybrene (Sigma-Aldrich) was added to the medium to a final concentration of 8 μg/ml. Cells were analyzed using flow cytometry 48 h after transduction, and percentage of the cells expressing RFP was used to calculate the number of transducing units (TU) per ml. To infect A549 and HaCaT cells, 1 ml of viral particles with concentration of at least $10^7$ TU/ml were added to $5\times10^6$ cells in 2 ml of culture medium, and the medium was replaced with fresh medium after 24 h. Infected cells were grown in the presence of 0.1% (v/v) of puromycin (Thermo Fischer Scientific, USA) followed by fluorescence-activated sorting based on RFP fluorescence intensity (excitation 561 nm, emission 585/15 nm BP) using a FACSAria SORP cell sorter (BD Biosciences, USA) with a 85 um nozzle and corresponding pressure parameters. After obtaining cell line with stable expression of vinculin-RFP, HaCaT-RFP or A549-RFP cells with medium fluorescence level in the RFP-PE channel (27% of events with MFI 1.68) were sorted out and cells with high RFP fluorescence (15.5% of events with MFI 18.77) were excluded. We also compared the levels of expression of vinculin mRNA in these cells with non-infected cells and find no statistically significant differences, confirming that the RFP- expressing cells have physiological level of vinculin expression (Fig. S1 in the Online Resource 1).

**Immunofluorescence.** Cells with stable expression of RFP-conjugated vinculin, A549-vin-RFP or HaCaT-vin-RFP, were fixed in a 4% PFA (paraformaldehyde) solution for 15 min at room temperature (RT). After 3 washes with PBS (phosphate buffered saline) and permeabilization of cells with a mixture of 0.01% Triton-X100 and 0.01% Tween-20 (Amresco, USA) in PBS for 60 min at RT, nonspecific antibody binding was next blocked by incubating cells for 1 h in a 5% BSA (Sigma-Aldrich) solution. Then cells were incubated with primary recombinant anti-paxillin antibodies (produced in rabbit, clone Y113, Abcam, UK) at final dilution of 1 : 200 at 37°C for 60 min followed by incubation with secondary anti-rabbit antibodies conjugated with Alexa-633 (Abcam) at a final dilution of 1 : 200 and co-stained with DAPI (Sigma-Aldrich) for nuclei visualization. Images were captured using a Zeiss AxioObserver with a LED light source Colibry 7 and objective PlanApochromat 63×1.46 Oil. The following filter cube was used: GFP (excitation filter 450-490 nm, a beam splitter 495 nm, emission 500-550 nm) and mKate (excitation filter 540-580 nm, a beam splitter 585 nm, emission 593-668 nm). Data were processed with the Zeiss Zen Blue 3.1 software.

**Inhibitory analysis.** To inactivate FAK, A549-vin-RFP or HaCaT-vin-RFP cells were treated with 1 μM of selective FAK inhibitor PF-573228 (Selleck, USA) for 2 h prior to analysis, inhibitor was not washed out before microscopy.

**Image analysis.** Microscopy data were analyzed using ImageJ program (NIH) [26]. FA area, aspect ratio, and lifetime values were measured and calculated for FAs as described in Gladkikh et al. [27]; a dataset of 200 to 500 focal adhesions was analyzed for each experimental point. Mean fluorescence intensity (MFI) was used as an indirect indicator of the amount of target protein in FA. Fluorescence images were processed using Adobe Photoshop (Adobe Systems, USA) software.

**Statistics.** Statistical analysis was performed using the GraphPad Prism7 software (GraphPad Software, USA). Mann–Whitney test was used to compare differences between two independent groups, the $p$-value < 0.05 was considered as significant. Data are presented as a median with range for FA parameters or as a mean ± SD for mRNA expression and wound healing assay.

## RESULTS

**FA size depends on the substrate and correlates with the wound closure rate.** In the control HaCaT cells and A549 cells cultivated on the chemically clear glass and located at the edge of the monolayer, FAs were localized mostly at the cell edge for both model cell lines (Fig. 1a). FAs in the A549 cell line on the glass have the median area of 1.17 μm$^2$ (range 0.11-5.33, $n$ = 500) and typically are of ellipsoidal shape (median aspect ratio is 1.73, range 1.0-5.54). FAs in the HaCaT cells have similar median area (0.98 μm$^2$, range 0.12-8.36), but are much more elongated (median aspect ratio is 2.46, range 1.02-7.09, $n$ = 500).

To evaluate relationship between the FA descriptors and cell motility we performed the wound healing assay as a gold standard for analysis of epithelial cells migration. To modify the size of FAs we used

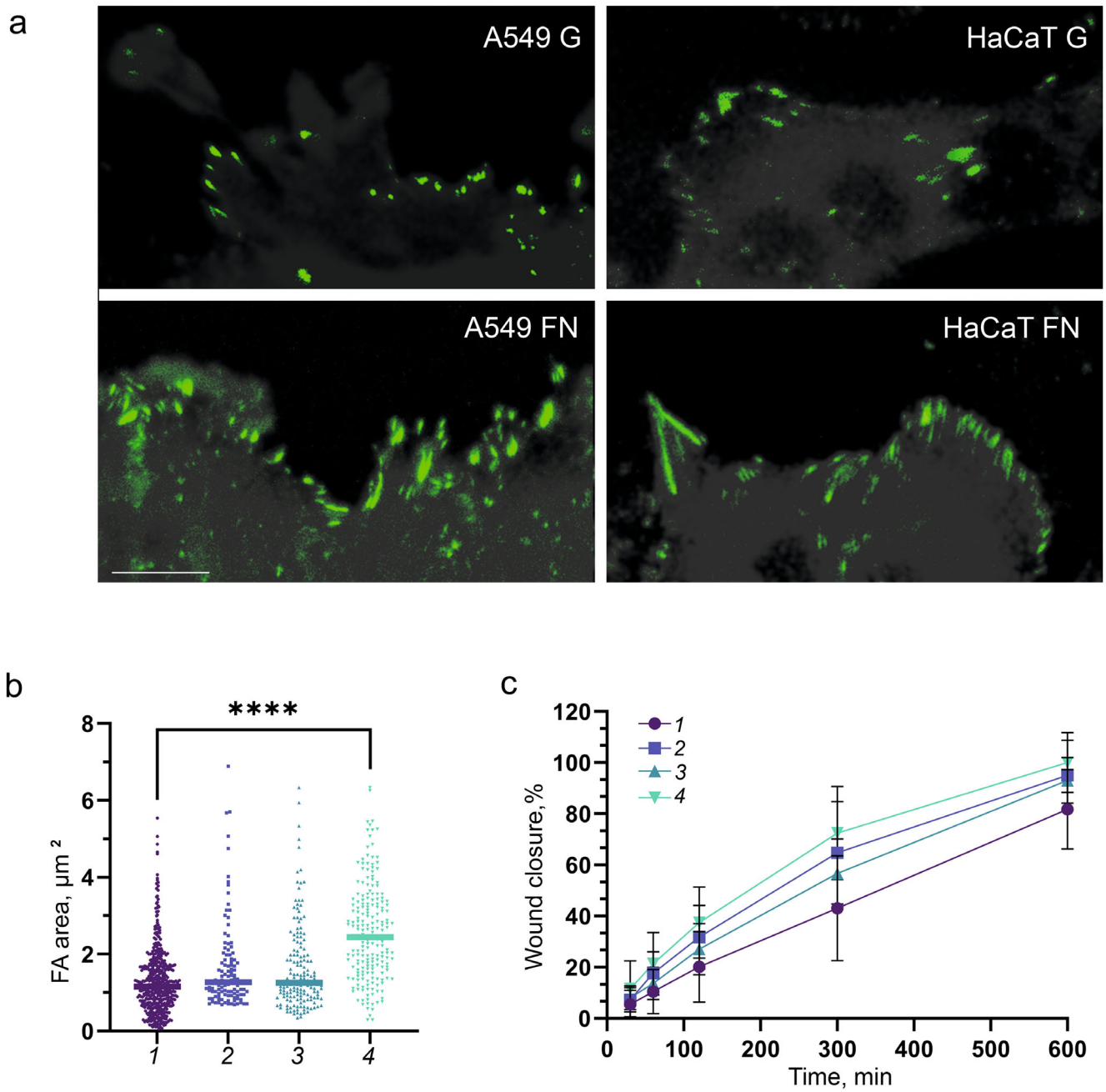


**Fig. 1.** FA morphology correlates with the wound closure rate on substrates with different stiffness. a) Morphology of FAs in A549 and HaCaT cells with stable expression of vinculin–RFP; scale bar 10 μm; designations: G, glass; FN, fibronectin; cells at the edge of monolayer are visualized. b) Median FA area of A549 cells on substrates with different stiffness, central horizontal line represents median. **** Difference from the control is statistically significant, $p < 0.0001$; c) Wound closure rate in % from the initial area on the first frame for A549 cells on glass (*1*), poly-D-lysine (*2*), vitronectin (*3*), and fibronectin (*4*).

substrates of varying stiffness (glass, poly-D-lysine, vitronectin, and fibronectin). For both cell lines the cells on fibronectin had the largest FA median area: 2.44 μm² for A549 (range 0.29-6.05), 1.32 μm² for HaCaT (range 0.11-7.37) (Fig. 1b, Fig. S2 in the Online Resource 1), while the median FA area for the cells on glass was the smallest (median area 1.22 μm² for A549, 0.99 μm² for HaCaT) ($p < 0.0001$ for A549, $p = 0.0002$ for HaCaT, Mann–Whitney test).

Wound closure rate also varied in accordance with the used substrate. For both cell lines the highest migration rate was observed on fibronectin, where FAs were the largest. We obtained 100 ± 11.75% of wound closure within 600 min for the A549 cells and 61.74 ± ± 16.88% for the HaCaT cells on fibronectin. Cells on glass had the lowest migration rate (81.70 ± 15.54% of wound closure for A549 cells, 43.95 ± 13.31% for HaCaT cells), cells on vitronectin and poly-L-lysine had inter-

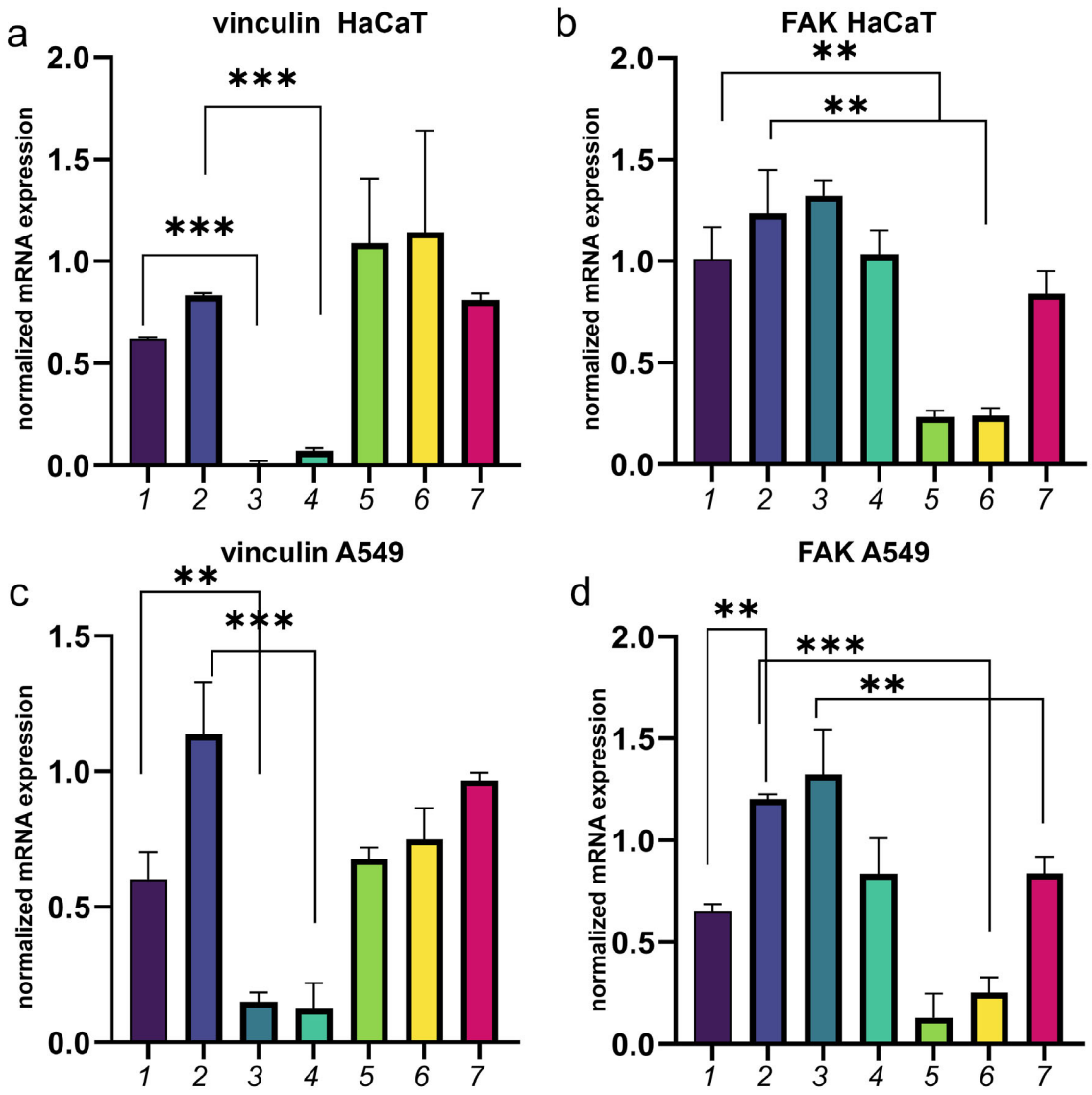


**Fig. 2.** Normalized mRNA expression of vinculin (a, c) and FAK (b, d) in the A549 cells and in the control HaCaT cells and after depletion of vinculin or FAK. All measurements were made in 3 biological replicates, data were normalized to UBC and HPRT1 genes. Designations: *1*) control cells on glass, *2*) control cells on fibronectin, *3*) cells with siRNA to vinculin on glass, *4*) cells with siRNA to vinculin on fibronectin, *5*) cells with siRNA to FAK on glass, *6*) cells with siRNA to FAK on fibronectin, *7*) cells with siRNA to GFP. ** Significant difference from the control, $p < 0.01$; *** significant difference from the control, $p < 0.001$

mediate migration rates (Fig. 1b, Fig. S3 in the Online Resource 1).

Next, we assessed which FA components are responsible for the FA area increase on different substrates. For that, we measured overall mRNA expression of vinculin (as a structural protein) and FAK (as a regulatory protein) and found upregulated vinculin expression in the A549 and HaCaT cells grown on fibronectin for 72 h compared to the cells grown on glass. Vinculin mean relative mRNA quantity in the A549 cells was 1.14 ± 0.19 on fibronectin compared to 0.60 ± ± 0.10 on glass, for the HaCaT cells it was 0.83 ± 0.01 on fibronectin vs 0.62 ± 0.01 on glass, though the differences were statistically insignificant (Fig. 2, a, c). FAK mRNA expression was also upregulated in the cells cultivated on fibronectin (mean relative mRNA quantity 0.77 ± 0.05 vs 1.18 ± 0.03 for A549 cells and 0.95 ± ± 0.15 vs 1.23 ± 0.21 for HaCaT cells) compared to the cells cultivated on glass (Fig. 2, b, d) (differences were statistically significant only for the A549 cells, $p = 0.03$, nonparametric Mann–Whitney test). Since upregulated expression of these proteins on fibronectin correlated with the increased cell motility, we sought to define whether altering expression of these proteins could change the cell motility parameters.

**Downregulation of vinculin expression decreases the size of FAs, but does not affect cell motility descriptors.** To examine the role of altered vinculin

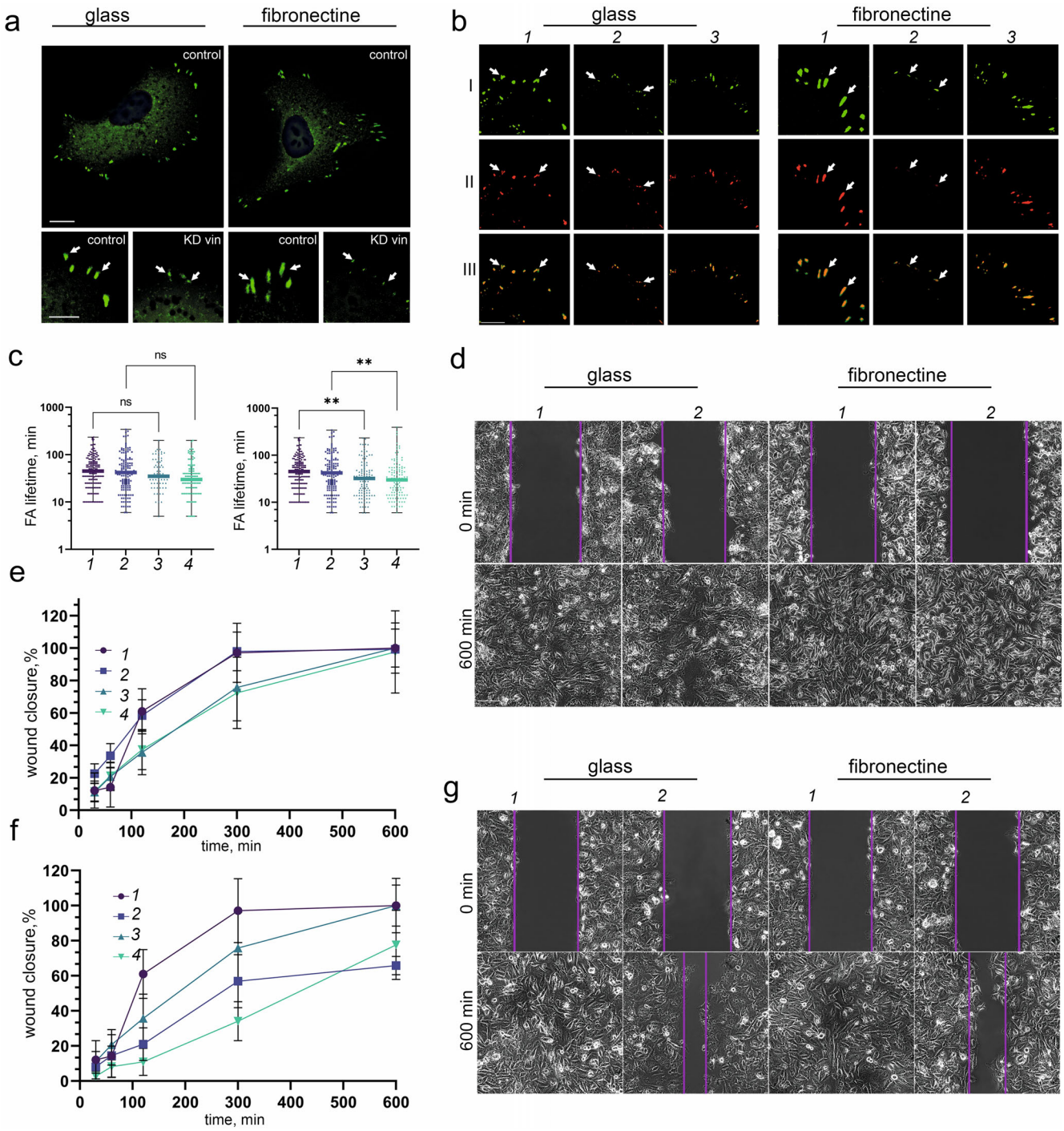


**Fig. 3.** FA parameters and rate of wound healing by the A549 cells after suppression of FAK or vinculin mRNA expression. a) Morphology of focal adhesions in the cells on glass and fibronectin in the control and after vinculin knockdown (KD vin); scale bar: 10 μm. b) Staining of the fixed A549 cells with stable vinculin RFP expression with antibodies to paxillin. Designations: *1*) control, *2*) cells with siRNA to vinculin, *3*) cells with siRNA to FAK, I) staining with antibodies to vinculin, II) staining with antibodies to paxillin, III) overlay. c) Lifetime of FAK in A549 cells, bold horizontal lines represent medians. Designations: *1*) control cells on fibronectin, *2*) control cells on glass, *3*) cells with siRNA to vinculin on fibronectin, *4*) cells with siRNA to vinculin on glass. ** Significant difference from the control, $p < 0.01$. d) Morphology of wound closure by the A549 cells on fibronectin and on glass in the control (*1*) and after vinculin knockdown (*2*). e) Wound closure rate in % of area at the first frame for the A549 cells on fibronectin in the control (*1*), on fibronectin in the cells with siRNA to vinculin (*2*), on glass in the control (*3*) and on glass in the cells with siRNA to vinculin (*4*). f) Wound closure rate in % of area at the first imaging frame for the A549 cells on fibronectin in the control (*1*), on fibronectin in the cells with siRNA to FAK (*2*), on glass in the control (*3*) and on glass in the cells with siRNA to FAK (*4*). g) Morphology of wound closure by the A549 cells on fibronectin and on glass in the control (*1*) and after FAK knockdown (*2*). The number of experiments for each wound scratch assay is given in Table S3 in the Online Resource 1.

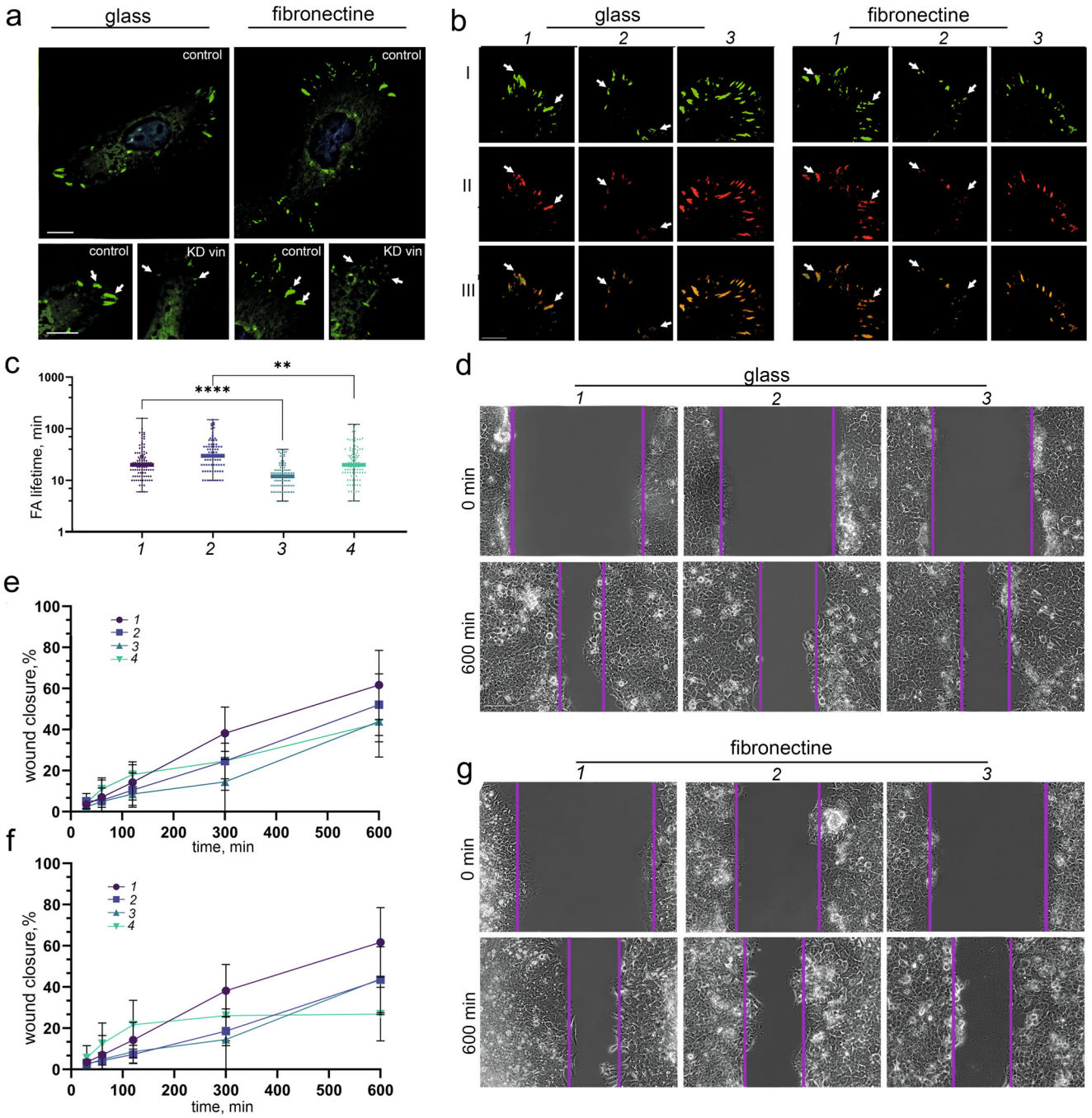


**Fig. 4.** FA parameters and wound healing rate by the HaCaT cells after suppression of FAK or vinculin mRNA expression. a) Morphology of focal adhesions on glass and fibronectin in the control cells and after vinculin knockdown (KD vin); scale bar: 10 μm. b) Staining of the fixed HaCaT cells with stable vinculin RFP expression with antibodies to paxillin, *1*) control, *2*) cells with siRNA to vinculin, *3*) cells with siRNA to FAK, I) staining with antibodies to vinculin, II) staining with antibodies to paxillin, III) overlay. c) Lifetime of FAK in the HaCaT cells, bold horizontal lines represent medians. Designations: *1*) control cells on fibronectin, *2*) control cells on glass, *3*) cells with siRNA to FAK on fibronectin, *4*) cells with siRNA to FAK on glass; ** significant difference from the control, $p < 0.01$; **** significant difference from the control, $p < 0.0001$. d) Morphology of wound closure by the HaCaT cells on glass in the control (*1*), after vinculin knockdown (*2*), and after FAK knockdown (*3*). e) Wound closure rate in % of area at the first imaging frame for the A549 cells on fibronectin in the control (*1*), on fibronectin in the cells with siRNA to vinculin (*2*), on glass in the control (*3*) and on glass in the cells with siRNA to vinculin (*4*). f) Wound closure rate in % of area on the first imaging frame for the HaCaT cells on fibronectin in the control (*1*), on fibronectin in the cells with siRNA to FAK (*2*), on glass in the control (*3*) and on glass in the cells with siRNA to FAK (*4*). g) Morphology of experimental wound overgrowth by the HaCaT cells on fibronectin and on glass in the control (*1*) after vinculin knockdown (*2*), and after FAK knockdown (*3*). The number of experiments for each wound scratch assay is shown in Table S3 in the Online Resource 1.

expression in cell migration, we depleted vinculin by siRNA treatment. We obtained 4 to 10-fold downregulation of the vinculin expression for the A549 cells and 10 to 60-fold downregulation of the vinculin expression in the HaCaT cells (Fig. 2, a, c). Downregulated expression levels of vinculin in the experiments fell within the physiological range for this protein, as cells retained their ability to migrate on the substrate, were capable of long-range movement (more than 10 nucleus diameters), and retained the overall normal morphology (Figs. 3a and 4a).

Downregulation of vinculin expression in the A549 cells cultivated on glass led to 2.6-fold decrease in the area of FAs (median FA area 0.45 μm$^2$ compared to 1.17 μm$^2$ in control) and to 4.8-fold decrease in the median fluorescence intensity (from 417 a.u. in the control to 87 a.u. in the vinculin-depleted cells), but did not change the aspect ratio (median aspect ratio (AR) 1.79 compared to 1.73 in the control). The FA area decrease after vinculin depletion was statistically significant both for the A549 and HaCaT cells ($p < 0.0001$, nonparametric Mann–Whitney test, Fig. S4 in the Online Resource 1). Downregulation of vinculin expression in the HaCaT cells also led to 2-fold decrease in the FA area (median FA area from 0.98 μm$^2$ to 0.55 μm$^2$), the median fluorescence intensity also decreased from 372 a.u. in the control to 205 a.u. in the vinculin-depleted cells. We have confirmed reduction of the FA area by staining the vinculin-depleted cells with the antibodies to paxillin as an alternative FA reporter protein (Figs. 3b and 4b). FA lifetime did not change after depletion of the vinculin mRNA expression (Figs. 3c and 4c).

To evaluate impact of the altered vinculin expression on cell migration, we used the wound healing assay. In this assay downregulation of the vinculin expression in the HaCaT and A549 cells did not significantly decrease the wound closure rate both on glass and fibronectin (Figs. 3d and 4d). For the vinculin-depleted A549 cells the wound closure in 600 min was 99.29 ± 2.45% on fibronectin and 97.70 ± 25.34% on glass, which is similar to the control values (Fig. 3d). For the HaCaT cells the wound closure in 600 min was 52.16 ± 15.0% on fibronectin and 43.19 ± 9.18% on glass, which is also close to the control (Fig. 4d). In the control, both on glass and fibronectin the cell front (leading edge) was straight. After 3 h individual cells detached from the cell front and began to migrate into the wound. Direction of the individual cell migration was in line with the direction of the cell front migration. After the vinculin expression reduction even at the early stage of wound closure (within 3 h) the cell front of the wound edge became rutted and uneven. Movement of the cells in the layer became uncoordinated. After 3 h the cells left the monolayer and continued to move chaotically along the border of the monolayer (lateral migration) (Fig. S5 in the Online Resource 1).

**FAK depletion dramatically alters motility of the normal and cancer epitheliocytes in the wound healing assay.** To verify the effect of alteration in FAK expression on FA parameters and cell motility, we also used siRNA treatment. Using specific siRNA resulted in 4-to 6-fold downregulation of FAK expression in the A549 cells and 3- to 4-fold FAK depletion in the HaCaT cells (Fig. 2, b, d). Depletion of FAK in the A549 cells did not affect neither the area, nor the aspect ratio of focal adhesions (median FA area was 1.11 μm$^2$, median AR was 1.84) (Fig. S4 in the Online Resource 1), depletion of FAK in the HaCaT cells also did not affect the FA morphology (median FA area 0.98, median AR 1.84) (Fig. 4a).

To confirm absence of the changes in FA area, we stained the FAK-depleted cells using the labeled antibodies against paxillin as an alternate FA reporter protein (Figs. 3b and 4b). The wound closure rate by the cells with low FAK expression was dramatically reduced. The A549 cells with depleted FAK cultivated on fibronectin closed the wound up to 65.84 ± 5.25% in 600 minutes (compared to 100 ± 11.75% in the control) (Fig. 3e). The same effect was observed for the HaCaT cells cultivated on fibronectin, as the wound closure was only 43.52 ± 16.06% compared to 61.74 ± 16.88% in the control (Fig. 4e). When the cells were cultivated on glass, the wound closure was 77.65 ± 19.68% in 600 min for the FAK-depleted A549 cells and 26.88 ± 13.04% for the FAK-depleted HaCaT cells. There were no significant differences in the cell morphology in the control cells and in the cells with FAK mRNA depletion; the overall wound edge remained flat throughout the time of imaging (Figs. 3g and 4g). Notably, we found a statistically significant decrease of the FA lifetime for the FAK-depleted cells of both cell lines. For the A549 cells the median FA lifetime decreased from 45 to 32 min on fibronectin and from 42 to 30 min on glass (Fig. 3c). For the HaCaT cells the median FA lifetime decreased fro m 20 to 12 min on fibronectin and from 30 to 20 min on glass (Fig. 4c).

To verify this finding, we used selective FAK kinase inhibitor PF-573228 and assessed the effect of FAK inhibition on the FA parameters and wound closure rate. Incubation of the cells with 1 μM of PF-573228 did not affect the median FA area of HaCaT and A549 cells, as well as the aspect ratio and fluorescence intensity (data not shown), but dramatically decreased the wound closure rate. Wound closure on glass for the A549 cells with inhibited FAK was only 59.42 ± 5.69% and only 19.26 ± 7.48% for the HaCaT cells. The wound closure by the cells with inhibited FAK cultivated on fibronectin was only 77.87 ± 3.77% for the A549 cells and 30.15 ± 5.86% for the HaCaT cells (Fig. 5).

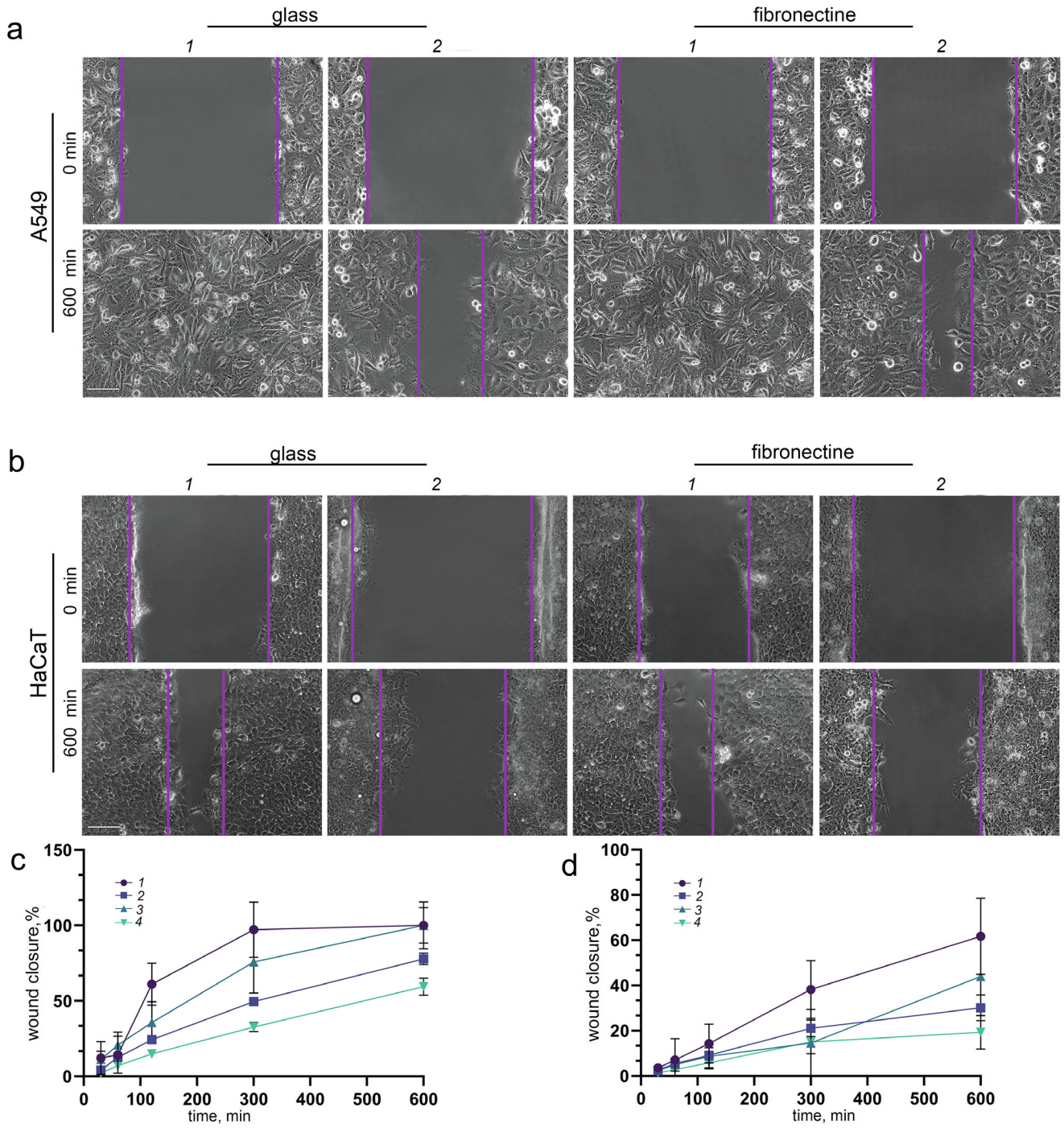


**Fig. 5.** a) Wound closure by the A549 cells cultivated on fibronectin and on glass in the control (*1*) and after incubation with 1 μM PF 573228 (*2*). b) Wound closure by the HaCaT cells cultivated on fibronectin and on glass in the control (*1*) and after incubation with 1 μM PF 573228 (*2*). c) Wound closure rate in % of area in the first imaging frame for the A549 cells cultivated on fibronectin in the control cells (*1*), cells cultivated on fibronectin after incubation with 1 μM PF 573228 (*2*), cells cultivated on glass in the control (*3*), and cells cultivated on glass after incubation with 1 μM PF 573228 (*4*). d) Wound closure rate in % of area at the first imaging frame for the HaCaT cells cultivated on fibronectin in the control cells (*1*), cells cultivated on fibronectin after incubation with 1 μM PF 573228 (*2*), cells cultivated on glass in the control (*3*) and cultivated on glass after incubation with 1 μM PF 573228 (*4*).

## DISCUSSION

FAK kinase, initially considered as a key regulatory molecule of integrin signaling pathway, is pivotal for cell migration and invasion [28, 29]; to date its roles in cell survival, angiogenesis, and fine tuning of tumor environment are established [30-32]. Due to the critical impact of FAK signaling in cancer progression,

this molecule is one of the most promising targets for anti-cancer therapy.

Most FAK inhibitors are competitive or allosteric molecules that block kinase catalytic activity of FAK [33-35]. Inhibition of FAK signaling pathway reduced both primary and secondary tumor growth in the mouse breast cancer models [36], inhibited motility of the pancreatic adenocarcinoma cells [37], and suppressed cell proliferation or even induced cell senescence in the lung cancer cell lines [37]. Major mechanisms through which FAK facilitates cancer cell motility and metastasis are associated with formation of the dynamic FAs and actin cytoskeleton remodeling [38, 39]. Critical steps of cytoskeleton remodeling through FAK signaling include cross-activation of Src kinases [40], recruitment of talin and paxillin to FA sites [7, 41] together with activation of small GTPases signaling pathway that finally results in actin cytoskeleton reorganization and change of the cell migration pattern [42, 43]. FAK also acts as an important part of mechanotransduction process adjusting its activation level to the ECM stiffness [44, 45]. Both the increased ECM stiffness and density of integrin ligands promote β1 integrin-FAK signaling, which, in turn, activates the RhoA pathway, actin remodeling thus facilitating cell migration. Hence, ECM composition should be considered as an additional risk factor of the FAK-dependent tumor progression [46, 47].

Interrelation between the ECM composition, FAK activation, and changes in the cancer cells migratory potential was a subject of active research in recent decades [48, 49]. For a long time, the size of FAs has been considered as a key indicator of any extracellular or intracellular stimulus (e.g., substrate elasticity or cytoskeleton rearrangement) that regulates the rate of cell movement. Several studies have shown correlation between the FA size and cell migration parameters [22, 23, 50], however, the issue of FA dynamics in the cells moving directionally as part of a monolayer is still poorly understood.

Our current findings indicate that downregulation of vinculin expression leads to the substantial decrease in the size of FAs but does not significantly affect movement of the epithelial cells in monolayer, though a lot of chaotically migrating non-polarized cells appear in the wound (Fig. S5 in the Online Resource 1). This is in line with the previous observations that vinculin plays a key role in polarization and persistent cell movement, and its depletion results in repeated reversal of migration direction [51]. It was shown using the model of a subcofluent monolayer of MDCK cells that translocation of vinculin between the intercellular and focal contacts serves as a regulator for switching between collective and single-cell migration [52], which is consistent with our data that the suppression of vinculin expression leads to its disappearance first of all from the intercellular contacts, and, as a result, the mechanism of collective migration is disrupted and individual migrating cells appear.

In contrast to vinculin, FAK depletion does not affect the size of FAs, but significantly slows down movement of the epithelial cell layer as observed for the normal keratinocytes and lung cancer cells, which is in agreement with other studies showing that FAK inactivation significantly reduces the rate of cell movement [8, 53]. Interestingly, the effect of FAK knockdown on the rate of cell movement is much less dramatic when evaluated in a random walk model [54, 55], that may reflect a key difference between the migration of cells in a layer and motility of individual cells.

Notably, we observed a statistically significant reduction of the FA lifetime in the FAK-depleted cells. According to the literature, FAK kinase facilitates turnover of FAs [56, 57] through fine tuning of the dynamics of other regulatory proteins [40, 58]. Cells with inactivated or absent FAK were reported to have decreased disassembly times and significantly longer FA lifetimes [35, 50]. It is also known that in the cells with reduced expression of FAK kinase, the number of stress fibrils is reduced, and the network of actin filaments becomes more homogeneous, resulting in a slower spreading process [59].

However, most of these observations were made on individual cells in a 2D random walk or a 3D migration model, whereas the model of collective cell migration cannot be modeled by migration of a group of isolated cells whose direction and speed of movement coincided unpredictably [60]. Wound healing assay is based on coordinated interaction of cells within a group, so that the speed and direction of movement of each individual cell directly depends on the movement of its neighbors [61]. For the normal keratinocyte cell line HaCaT and for the A549 adenocarcinoma tumor cells, we have shown that the FAK knockdown in the cells within a monolayer results in a significant decrease in the FA lifetime for both cells cultivated on glass and on fibronectin as substrate.

## CONCLUSION

Our data indicate that the FA area is not as critical as the FA lifetime for generation of the maximal cell migration speed in a monolayer. The short-living FAs apparently fail to adhere in due time and fail to create effective tension to move the layer forward, though this conclusion has to be proved in future in the assays with direct measurement of traction forces for the cell layers moving on flexible (wrinkling) substrates.

**Supplementary information.** The online version contains supplementary material available at https://doi.org/10.1134/S0006297924030088.

**Acknowledgments.** The authors acknowledge support from the MSU Program of Development (cell sorting experiments – FACSAria SORP cell sorter).

**Contributions.** I.A.V. and A.A.S. concept and supervision of the work; E.S.S., A.V.K., and A.A.S. performing experiments; E.S.S., A.V.K., and A.V.T. data analysis and image preparation; E.S. S. and A.A.S. writing the paper draft; A.A.S. and I.A.V. editing text of the manuscript.

**Funding.** This work was financially supported by the Russian Science Foundation (grant no. 22-24-00714).

**Ethics declarations.** This work does not contain any studies involving human and animal subjects. The authors of this work declare that they have no conflicts of interest.

## REFERENCES

1. Winograd-Katz, S. E., Fässler, R., Geiger, B., and Legate, K. R. (2014) The integrin adhesome: from genes and proteins to human disease, *Nat. Rev. Mol. Cell Biol.*, **15**, 273-288, doi: 10.1038/nrm3769.
2. Chastney, M. R., Lawless, C., Humphries, J. D., Warwood, S., Jones, M. C., Knight, D., Jorgensen, C., and Humphries, M. J. (2020) Topological features of integrin adhesion complexes revealed by multiplexed proximity biotinylation, *J. Cell. Biol.*, **219**, e202003038, doi: 10.1083/jcb.202003038.
3. Paszek, M. J., DuFort, C. C., Rubashkin, M. G., Davidson, M. W., Thorn, K. S., Liphardt, J. T., and Weaver, V. M. (2012) Scanning angle interference microscopy reveals cell dynamics at the nanoscale, *Nat. Methods*, **9**, 825-827, doi: 10.1038/nmeth.2077.
4. Stubb, A., Guzmán, C., Närvä, E., Aaron, J., Chew, T.-L., Saari, M., Miihkinen, M., Jacquemet, G., and Ivaska, J. (2019) Superresolution architecture of cornerstone focal adhesions in human pluripotent stem cells, *Nat. Commun.*, **10**, 4756, doi: 10.1038/s41467-019-12611-w.
5. Kleinschmidt, E. G., and Schlaepfer, D. D. (2017) Focal adhesion kinase signaling in unexpected places, *Curr. Opin. Cell. Biol.*, **45**, 24-30, doi: 10.1016/j.ceb.2017.01.003.
6. Schaller, M. D., and Parsons, J. T. (1995) pp125$^{FAK}$-dependent tyrosine phosphorylation of paxillin creates a high-affinity binding site for Crk, *Mol. Cell. Biol.*, **15**, 2635-2645, doi: 10.1128/MCB.15.5.2635.
7. López-Colomé, A. M., Lee-Rivera, I., Benavides-Hidalgo, R., and López, E. (2017) Paxillin: a crossroad in pathological cell migration, *J. Hematol. Oncol.*, **10**, 50, doi: 10.1186/s13045-017-0418-y.
8. Richardson, A., Malik, R. K., Hildebrand, J. D., and Parsons, J. T. (1997) Inhibition of cell spreading by expression of the C-terminal domain of focal adhesion kinase (FAK) is rescued by coexpression of Src or catalytically inactive FAK: a role for paxillin tyrosine phosphorylation, *Mol. Cell. Biol.*, **17**, 6906-6914, doi: 10.1128/MCB.17.12.6906.
9. Fan, T., Chen, J., Zhang, L., Gao, P., Hui, Y., Xu, P., Zhang, X., and Liu, H. (2016) Bit1 knockdown contributes to growth suppression as well as the decreases of migration and invasion abilities in esophageal squamous cell carcinoma via suppressing FAK-paxillin pathway, *Mol. Cancer*, **15**, 23, doi: 10.1186/s12943-016-0507-5.
10. Schlaepfer, D. D., Mitra, S. K., and Ilic, D. (2004) Control of motile and invasive cell phenotypes by focal adhesion kinase, *Biochim. Biophys. Acta*, **1692**, 77-102, doi: 10.1016/j.bbamcr.2004.04.008.
11. Wang, S., Hwang, E. E., Guha, R., O'Neill, A. F., Melong, N., Veinotte, C. J., Conway Saur, A., Wuerthele, K., Shen, M., McKnight, C., Alexe, G., Lemieux, M. E., Wang, A., Hughes, E., Xu, X., Boxer, M. B., Hall, M. D., Kung, A., Berman, J. N., Davis, M. I., Stegmaier, K., and Crompton, B. D. (2019) High-throughput chemical screening identifies focal adhesion kinase and Aurora kinase B inhibition as a synergistic treatment combination in Ewing sarcoma, *Clin. Cancer Res.*, **25**, 4552-4566, doi: 10.1158/1078-0432.CCR-17-0375.
12. Demircioglu, F., Wang, J., Candido, J., Costa, A. S. H., Casado, P., De Luxan Delgado, B., Reynolds, L. E., Gomez-Escudero, J., Newport, E., Rajeeve, V., Baker, A.-M., Roy-Luzarraga, M., Graham, T. A., Foster, J., Wang, Y., Campbell, J. J., Singh, R., Zhang, P., Schall, T. J., Balkwill, F. R., Sosabowski, J., Cutillas, P. R., Frezza, C., Sancho, P., and Hodivala-Dilke, K. (2020) Cancer associated fibroblast FAK regulates malignant cell metabolism, *Nat. Commun.*, **11**, 1290, doi: 10.1038/s41467-020-15104-3.
13. Serrels, A., Lund, T., Serrels, B., Byron, A., McPherson, R. C., von Kriegsheim, A., Gómez-Cuadrado, L., Canel, M., Muir, M., Ring, J. E., Maniati, E., Sims, A. H., Pachter, J. A., Brunton, V. G., Gilbert, N., Anderton, S. M., Nibbs, R. J. B., and Frame, M. C. (2015) Nuclear FAK controls chemokine transcription, Tregs, and evasion of anti-tumor immunity, *Cell*, **163**, 160-173, doi: 10.1016/j.cell.2015.09.001.
14. Tavora, B., Reynolds, L. E., Batista, S., Demircioglu, F., Fernandez, I., Lechertier, T., Lees, D. M., Wong, P.-P., Alexopoulou, A., Elia, G., Clear, A., Ledoux, A., Hunter, J., Perkins, N., Gribben, J. G., and Hodivala-Dilke, K. M. (2014) Endothelial-cell FAK targeting sensitizes tumours to DNA-damaging therapy, *Nature*, **514**, 112-116, doi: 10.1038/nature13541.
15. You, D., Xin, J., Volk, A., Wei, W., Schmidt, R., Scurti, G., Nand, S., Breuer, E.-K., Kuo, P. C., Breslin, P., Kini, A. R., Nishimura, M. I., Zeleznik-Le, N. J., and Zhang, J. (2015) FAK mediates a compensatory survival signal parallel to PI3K-AKT in PTEN-Null T-all cells, *Cell Rep.*, **10**, 2055-2068, doi: 10.1016/j.celrep.2015.02.056.
16. Adutler-Lieber, S., Zaretsky, I., Platzman, I., Deeg, J., Friedman, N., Spatz, J. P., and Geiger, B. (2014) Engineering of synthetic cellular microenvironments:

implications for immunity, *J. Autoimmun.*, **54**, 100-111, doi: 10.1016/j.jaut.2014.05.003.
17. Cavalcanti-Adam, E. A., Volberg, T., Micoulet, A., Kessler, H., Geiger, B., and Spatz, J. P. (2007) Cell spreading and focal adhesion dynamics are regulated by spacing of integrin ligands, *Biophys. J.*, **92**, 2964-2974, doi: 10.1529/biophysj.106.089730.
18. Chiu, C.-L., Aguilar, J. S., Tsai, C. Y., Wu, G., Gratton, E., and Digman, M. A. (2014) Nanoimaging of focal adhesion dynamics in 3D, *PLoS One*, **9**, e99896, doi: 10.1371/journal.pone.0099896.
19. Engler, A. J., Sen, S., Sweeney, H. L., and Discher, D. E. (2006) Matrix elasticity directs stem cell lineage specification, *Cell*, **126**, 677-689, doi: 10.1016/j.cell.2006.06.044.
20. Doyle, A. D., Carvajal, N., Jin, A., Matsumoto, K., and Yamada, K. M. (2015) Local 3D matrix microenvironment regulates cell migration through spatiotemporal dynamics of contractility-dependent adhesions, *Nat. Commun.*, **6**, 8720, doi: 10.1038/ncomms9720.
21. Yue, J., Zhang, Y., Liang, W. G., Gou, X., Lee, P., Liu, H., Lyu, W., Tang, W.-J., Chen, S.-Y., Yang, F., Liang, H., and Wu, X. (2016) In vivo epidermal migration requires focal adhesion targeting of ACF7, *Nat. Commun.*, **7**, 11692, doi: 10.1038/ncomms11692.
22. Kim, D., and Wirtz, D. (2013) Focal adhesion size uniquely predicts cell migration, *FASEB J.*, **27**, 1351-1361, doi: 10.1096/fj.12-220160.
23. Thompson, O., Moore, C. J., Hussain, S.-A., Kleino, I., Peckham, M., Hohenester, E., Ayscough, K. R., Saksela, K., and Winder, S. J. (2010) Modulation of cell spreading and cell-substrate adhesion dynamics by dystroglycan, *J. Cell. Sci.*, **123**, 118-127, doi: 10.1242/jcs.047902.
24. Kauanova, S., Urazbayev, A., and Vorobjev, I. (2021) The frequent sampling of Wound scratch assay reveals the "opportunity" window for quantitative evaluation of cell motility-impeding drugs, *Front. Cell Dev. Biol.*, **9**, 640972, doi: 10.3389/fcell.2021.640972.
25. Vandesompele, J., Preter, K. D., Roy, N. V., and Paepe, A. D. (2002) Accurate normalization of real-time quantitative RT-PCR data by geometric averaging of multiple internal control genes, *Genome Biol.*, **3**, research0034.1, doi: 10.1186/gb-2002-3-7-research0034.
26. Abramoff, M. D., Magalhaes, P. J., and Ram, S. J. (2004) Image processing with ImageJ, *Biophotonics Int.*, **11**, 36-42.
27. Gladkikh, A., Kovaleva, A., Tvorogova, A., and Vorobjev, I. A. (2018) Heterogeneity of focal adhesions and focal contacts in motile fibroblasts, *Methods Mol. Biol.*, **1745**, 205-218, doi: 10.1007/978-1-4939-7680-5_12.
28. Guan, J. L., Trevithick, J. E., and Hynes, R. O. (1991) Fibronectin/integrin interaction induces tyrosine phosphorylation of a 120-kDa protein, *Cell. Regul.*, **2**, 951-964, doi: 10.1091/mbc.2.11.951.
29. Kornberg, L., Earp, H. S., Parsons, J. T., Schaller, M., and Juliano, R. L. (1992) Cell adhesion or integrin clustering increases phosphorylation of a focal adhesion-associated tyrosine kinase, *J. Biol. Chem.*, **267**, 23439-23442, doi: 10.1016/S0021-9258(18)35853-8.
30. Chuang, H.-H., Zhen, Y.-Y., Tsai, Y.-C., Chuang, C.-H., Hsiao, M., Huang, M.-S., and Yang, C.-J. (2022) FAK in cancer: from mechanisms to therapeutic strategies, *Int. J. Mol. Sci.*, **23**, 1726, doi: 10.3390/ijms23031726.
31. Golubovskaya, V. (2014) Targeting FAK in human cancer: from finding to first clinical trials, *Front. Biosci*, **19**, 687, doi: 10.2741/4236.
32. Rigiracciolo, D. C., Cirillo, F., Talia, M., Muglia, L., Gutkind, J. S., Maggiolini, M., and Lappano, R. (2021) Focal adhesion kinase fine tunes multifaced signals toward breast cancer progression, *Cancers*, **13**, 645, doi: 10.3390/cancers13040645.
33. Hirt, U. A., Waizenegger, I. C., Schweifer, N., Haslinger, C., Gerlach, D., Braunger, J., Weyer-Czernilofsky, U., Stadtmüller, H., Sapountzis, I., Bader, G., Zoephel, A., Bister, B., Baum, A., Quant, J., Kraut, N., Garin-Chesa, P., and Adolf, G. R. (2018) Efficacy of the highly selective focal adhesion kinase inhibitor BI 853520 in adenocarcinoma xenograft models is linked to a mesenchymal tumor phenotype, *Oncogenesis*, **7**, 21, doi: 10.1038/s41389-018-0032-z.
34. Kanteti, R., Mirzapoiazova, T., Riehm, J. J., Dhanasingh, I., Mambetsariev, B., Wang, J., Kulkarni, P., Kaushik, G., Seshacharyulu, P., Ponnusamy, M. P., Kindler, H. L., Nasser, M. W., Batra, S. K., and Salgia, R. (2018) Focal adhesion kinase a potential therapeutic target for pancreatic cancer and malignant pleural mesothelioma, *Cancer Biol. Ther.*, **19**, 316-327, doi: 10.1080/15384047.2017.1416937.
35. Slack-Davis, J. K., Martin, K. H., Tilghman, R. W., Iwanicki, M., Ung, E. J., Autry, C., Luzzio, M. J., Cooper, B., Kath, J. C., Roberts, W. G., and Parsons, J. T. (2007) Cellular characterization of a novel focal adhesion kinase inhibitor, *J. Biol. Chem.*, **282**, 14845-14852, doi: 10.1074/jbc.M606695200.
36. Tiede, S., Meyer-Schaller, N., Kalathur, R. K. R., Ivanek, R., Fagiani, E., Schmassmann, P., Stillhard, P., Häfliger, S., Kraut, N., Schweifer, N., Waizenegger, I. C., Bill, R., and Christofori, G. (2018) The FAK inhibitor BI 853520 exerts anti-tumor effects in breast cancer, *Oncogenesis*, **7**, 73, doi: 10.1038/s41389-018-0083-1.
37. Zhang, J., He, D.-H., Zajac-Kaye, M., and Hochwald, S. N. (2014) A small molecule FAK kinase inhibitor, GSK2256098, inhibits growth and survival of pancreatic ductal adenocarcinoma cells, *Cell Cycle*, **13**, 3143-3149, doi: 10.4161/15384101.2014.949550.
38. Katoh, K. (2020) FAK-dependent cell motility and cell elongation, *Cells*, **9**, 192, doi: 10.3390/cells9010192.
39. Murphy, J. M., Rodriguez, Y. A. R., Jeong, K., Ahn, E.-Y. E., and Lim, S.-T. S. (2020) Targeting focal adhesion kinase in cancer cells and the tumor microenvironment, *Exp. Mol. Med.*, **52**, 877-886, doi: 10.1038/s12276-020-0447-4.

40. Horton, E. R., Humphries, J. D., Stutchbury, B., Jacquemet, G., Ballestrem, C., Barry, S. T., and Humphries, M. J. (2016) Modulation of FAK and Src adhesion signaling occurs independently of adhesion complex composition, *J. Cell. Biol.*, **212**, 349-364, doi: 10.1083/jcb.201508080.
41. Lawson, C., Lim, S.-T., Uryu, S., Chen, X. L., Calderwood, D. A., and Schlaepfer, D. D. (2012) FAK promotes recruitment of talin to nascent adhesions to control cell motility, *J. Cell. Biol.*, **196**, 223-232, doi: 10.1083/jcb.201108078.
42. Huveneers, S., and Danen, E. H. J. (2009) Adhesion signaling – crosstalk between integrins, Src and Rho, *J. Cell. Sci.*, **122**, 1059-1069, doi: 10.1242/jcs.039446.
43. Kallergi, G., Agelaki, S., Markomanolaki, H., Georgoulias, V., and Stournaras, C. (2007) Activation of FAK/PI3K/Rac1 signaling controls actin reorganization and inhibits cell motility in human cancer cells, *Cell. Physiol. Biochem.*, **20**, 977-986, doi: 10.1159/000110458.
44. Bell, S., and Terentjev, E. M. (2017) Focal adhesion kinase: the reversible molecular mechanosensor, *Biophys. J.*, **112**, 2439-2450, doi: 10.1016/j.bpj.2017.04.048.
45. Zhou, D. W., Lee, T. T., Weng, S., Fu, J., and García, A. J. (2017) Effects of substrate stiffness and actomyosin contractility on coupling between force transmission and vinculin-paxillin recruitment at single focal adhesions, *Mol. Biol. Cell*, **28**, 1901-1911, doi: 10.1091/mbc.e17-02-0116.
46. Boyd, N. F., Li, Q., Melnichouk, O., Huszti, E., Martin, L. J., Gunasekara, A., Mawdsley, G., Yaffe, M. J., and Minkin, S. (2014) Evidence that breast tissue stiffness is associated with risk of breast cancer, *PLoS One*, **9**, e100937, doi: 10.1371/journal.pone.0100937.
47. Levental, K. R., Yu, H., Kass, L., Lakins, J. N., Egeblad, M., Erler, J. T., Fong, S. F. T., Csiszar, K., Giaccia, A., Weninger, W., Yamauchi, M., Gasser, D. L., and Weaver, V. M. (2009) Matrix crosslinking forces tumor progression by enhancing integrin signaling, *Cell*, **139**, 891-906, doi: 10.1016/j.cell.2009.10.027.
48. Hamidi, H., and Ivaska, J. (2018) Every step of the way: integrins in cancer progression and metastasis, *Nat. Rev. Cancer*, **18**, 533-548, doi: 10.1038/s41568-018-0038-z.
49. Su, C., Li, J., Zhang, L., Wang, H., Wang, F., Tao, Y., Wang, Y., Guo, Q., Li, J., Liu, Y., Yan, Y., and Zhang, J. (2020) The Biological Functions and Clinical Applications of Integrins in Cancers, *Front. Pharmacol.*, **11**, 579068, doi: 10.3389/fphar.2020.579068.
50. Llić, D., Furuta, Y., Kanazawa, S., Takeda, N., Sobue, K., Nakatsuji, N., Nomura, S., Fujimoto, J., Okada, M., Yamamoto, T., and Aizawa, S. (1995) Reduced cell motility and enhanced focal adhesion contact formation in cells from FAK-deficient mice, *Nature*, **377**, 539-544, doi: 10.1038/377539a0.
51. Rahman, A., Carey, S. P., Kraning-Rush, C. M., Goldblatt, Z. E., Bordeleau, F., Lampi, M. C., Lin, D. Y., García, A. J., and Reinhart-King, C. A. (2016) Vinculin regulates directionality and cell polarity in 2D, 3D matrix and 3D microtrack migration, *Mol. Biol. Cell*, **27**, 1431-1441, doi: 10.1091/mbc.E15-06-0432.
52. Bejar-Padilla, V., Cabe, J. I., Lopez, S., Narayanan, V., Mezher, M., Maruthamuthu, V., and Conway, D. E. (2022) α-Catenin-dependent vinculin recruitment to adherens junctions is antagonistic to focal adhesions, *Mol. Biol. Cell*, **33**, ar93, doi: 10.1091/mbc.E22-02-0071.
53. Iwanicki, M. P., Vomastek, T., Tilghman, R. W., Martin, K. H., Banerjee, J., Wedegaertner, P. B., and Parsons, J. T. (2008) FAK, PDZ-RhoGEF and ROCKII cooperate to regulate adhesion movement and trailing-edge retraction in fibroblasts, *J. Cell. Sci.*, **121**, 895-905, doi: 10.1242/jcs.020941.
54. Xiao, W., Jiang, M., Li, H., Li, C., Su, R., and Huang, K. (2013) Knockdown of FAK inhibits the invasion and metastasis of Tca-8113 cells *in vitro*, *Mol. Med. Rep.*, **8**, 703-707, doi: 10.3892/mmr.2013.1555.
55. Fraley, S. I., Feng, Y., Krishnamurthy, R., Kim, D.-H., Celedon, A., Longmore, G. D., and Wirtz, D. (2010) A distinctive role for focal adhesion proteins in three-dimensional cell motility, *Nat. Cell. Biol.*, **12**, 598-604, doi: 10.1038/ncb2062.
56. Giannone, G., Rondé, P., Gaire, M., Beaudouin, J., Haiech, J., Ellenberg, J., and Takeda, K. (2004) Calcium rises locally trigger focal adhesion disassembly and enhance residency of focal adhesion kinase at focal adhesions, *J. Biol. Chem.*, **279**, 28715-28723, doi: 10.1074/jbc.M404054200.
57. Webb, D. J., Donais, K., Whitmore, L. A., Thomas, S. M., Turner, C. E., Parsons, J. T., and Horwitz, A. F. (2004) FAK-Src signalling through paxillin, ERK and MLCK regulates adhesion disassembly, *Nat. Cell. Biol.*, **6**, 154-161, doi: 10.1038/ncb1094.
58. Von Wichert, G. (2003) Force-dependent integrin-cytoskeleton linkage formation requires downregulation of focal complex dynamics by Shp2, *EMBO J.*, **22**, 5023-5035, doi: 10.1093/emboj/cdg492.
59. Horikiri, Y., Shimo, T., Kurio, N., Okui, T., Matsumoto, K., Iwamoto, M., and Sasaki, A. (2013) Sonic hedgehog regulates osteoblast function by focal adhesion kinase signaling in the process of fracture healing, *PLoS One*, **8**, e76785, doi: 10.1371/journal.pone.0076785.
60. Mayor, R., and Etienne-Manneville, S. (2016) The front and rear of collective cell migration, *Nat. Rev. Mol. Cell Biol.*, **17**, 97-109, doi: 10.1038/nrm.2015.14.
61. Szabó, B., Szöllösi, G. J., Gönci, B., Jurányi, Zs., Selmeczi, D., and Vicsek, T. (2006) Phase transition in the collective migration of tissue cells: experiment and model, *Phys. Rev. E*, **74**, 061908, doi: 10.1103/PhysRevE.74.061908.